HD 179949b: A Close Orbiting Extrasolar Giant Planet with a stratosphere?

J.R. Barnes[1]⋆ Travis S. Barman[2], H.R.A. Jones[1], C.J. Leigh[3], A. Collier Cameron[4], R.J. Barber[5] and D.J. Pinfield[1]

[1] *Centre for Astrophysics Research, University of Hertfordshire, Hertfordshire AL10 9AB. UK.*
[2] *Lowell Observatory, Planetary Research Centre, 1400 West Mars Hill Road, Flagstaff, AZ 86001. USA*
[3] *Astrophysics Research Institute, Liverpool John Moores University, Birkenhead CH41 1LD. UK.*
[4] *SUPA, School of Physics and Astronomy, University of St Andrews, Fife KY16 9SS. UK.*
[5] *Departments of Physics and Astronomy, University College London, London WC1E 6BT. UK.*

ABSTRACT

We have carried out a search for the 2.14 μm spectroscopic signature of the close orbiting extrasolar giant planet, HD 179949b. High cadence time series spectra were obtained with the CRIRES spectrograph at VLT1 on two closely separated nights. Deconvolution yielded spectroscopic profiles with mean S/N ratios of several thousand, enabling the near infrared contrast ratios predicted for the HD 179949 system to be achieved.

Recent models have predicted that the hottest planets may exhibit spectral signatures in emission due to the presence of TiO and VO which may be responsible for a temperature inversion high in the atmosphere. We have used our phase dependent orbital model and tomographic techniques to search for the planetary signature under the assumption of an absorption line dominated atmospheric spectrum, where T and V are depleted from the atmospheric model, and an emission line dominated spectrum, where TiO and VO are present.

We do not detect a planet in either case, but the 2.120 μm - 2.174 μm wavelength region covered by our observations enables the deepest near infrared limits yet to be placed on the planet/star contrast ratio of any close orbiting extrasolar giant planet system. We are able to rule out the presence of an atmosphere dominated by absorption opacities in the case of HD 179949b at a contrast ratio of $F_p/F_* \sim 1/3350$, with 99 per cent confidence.

Key words: Line: profiles – Methods: data analysis – Techniques: spectroscopic – Stars: late-type – Stars: individual: HD 179949 – Stars: planetary systems

1 INTRODUCTION

Recent models (Burrows et al. 2008) have focused on the role of a parametrized stratospheric absorbing molecular species which leads to abundant molecules such as H_2O appearing in emission in certain wavelength bands. Similarly, Fortney et al. (2008) have more specifically investigated the effects of TiO and VO which absorb much of the incoming stellar radiation high in the atmospheres of the hottest CEGPs. Fortney et al. (2008) expect that HD 179949b belongs to this class of hot CEGPs where the absorbing species lead to a temperature inversion and the formation of a

stratosphere. It is claimed that such models give better agreement with multi-wavelength mid-infrared Spitzer observations for those CEGPs which are most highly irradiated. Systems such as HD 209458b (Burrows et al. 2007; Knutson et al. 2008), HD 149026b and v And are among those systems which possess atmospheres most consistent with the presence of temperature inversions.

In the near infrared, the strong 2.2 μm bump due to the presence of strong H_2O and CO molecular bands for 2.2 μm $< \lambda > 2.2$ μm may not be present in systems which exhibit a stratosphere (Burrows et al. 2008). This possibility was indicated by observations of HD 209458b (Richardson et al. 2003) which failed to detect the 2.2 μm bump in the atmosphere of HD 209458b. The weak H_2O and

⋆ E-mail: j.r.barnes@herts.ac.uk

CO absorption transitions close to 2.2 µm are rather seen in emission while the 2.2 µm F_p/F_* flux ratio is lower and flatter owing to a spectral energy distribution which more closely resembles that of a blackbody.

1.1   HD 179949 and its planet

The presence of a close orbiting planetary system around the $M_v = 4.09 \pm 0.04$ F8 dwarf star, HD 179949 was first reported by Tinney et al. (2001). Eggenberger et al. (2007) included HD 179949 in a search for stellar duplicity but found no companion star, indicating it to be a single star system. Further, a survey of stars known to harbour planets (Santos et al. 2004) revealed that the [Fe/H] $= 0.22 \pm 0.05$ dex for HD 179949b places it in the most common metallicity band, in a distribution significantly more metal rich than than for stars which are not known to harbour planets. The reported velocity amplitude induced by the planet on its parent star, at $K = 101.3 \pm 3.0$ km s^{-1}, with orbital period of 3.093 ± 0.001 d and orbital radius of 0.045 ± 0.004 placed it among the closest orbiting planets. More recently, Butler et al. (2006) have published revised system parameters as a result of further monitoring of the system, finding $K = 112.6 \pm 1.8$ km s^{-1}, $P = 3.092514 \pm 0.000032$ d and $a = 0.0443 \pm 0.0026$ AU in a low eccentricity ($e = 0.022 \pm 0.015$) orbit. By studying emission in the Ca II H & K lines, Shkolnik et al. (2003) found evidence for perturbation of the stellar magnetic field with a periodicity which coincides with the orbital period of HD 179949b while Wolf & Harmanec (2004) found the stellar rotation period of HD 179949 to be independent of the planetary orbital period, with $P_{rot} = 7.06549 \pm 0.00061$ d. With no transit of the system reported, a minimum mass of $Msini = 0.916 \pm 0.076$ $M_\odot$ is found. The time of inferior conjunction is given by an ephemeris of HJD $= 2451001.510 \pm 0.020$ d (Butler et al. 2006). Wittenmyer et al. (2007) found no evidence for long period objects in the HD 179949 system and reported updated system parameters which are consistent with those of Butler et al. (2006) at the 1-σ level.

Cowan et al. (2007) presented mid-infrared Spitzer observations of the HD 179949 system which revealed a phase dependent light curve in phase with the planet's orbit and with a relative peak-to-trough amplitude of 0.00141 at 8 µm. This implies that less than 21 per cent of the incident stellar radiation is recirculated to the night side of the planet and contrasts with the other systems in their study, HD 209458 and 51 Peg, which did not reveal photometric variation, suggesting a higher level of redistribution of incident energy. While these observations were used by Burrows et al. (2008) to compare model fits, the data carry sufficiently high uncertainties that they enable a number of models with varying degrees of heat redistribution, absorber opacity and inclination to give reasonable fits. A hint that this degeneracy may be partially broken comes from the similarity between HD 179949b and υ And b (Harrington et al. 2006), both showing only a small shift between the superior conjunction ephemeris and lightcurve maximum. This may indicate that heat is re-radiated without being carried downstream, as suggested by the results of Harrington et al. (2006, 2007), due to the presence of a hot stratosphere which inhibits advection in the lower atmosphere.

In this paper, we present 2.14 µm observations taken with the Cryogenic high-resolution InfraRed Échelle Spectrograph (CRIRES) at the Very Large Telescope and search for the signature of a planet which exhibits either absorption or emission features. We first describe observations and data extraction procedures (§2) before describing the method (§3) which involves searching for the faint planetary spectrum in a mean spectrum subtracted timeseries of spectra. A Gaussian matched filter mimics the radial velocity motion and varying strength of the planetary spectrum which is used to search for the best fitting model. The results are presented in §4 and discussed in §5.

2   OBSERVATIONS AND DATA REDUCTION

Observations of HD 179949 were made with CRIRES at the Nasmyth focus of the Very Large Telescope, Unit 1 (VLT1, Antu), on 2007 July 26/27 and August 03 and are presented in Table 1. Four 1024x1024 InSb Aladdin-3 arrays were used to obtain each spectrum in the wavelength range $\lambda\lambda = 21215 - 21740$ Å. Observations were made in ABBA nodding sequences to enable subtraction of sky background and lines and to remove the effects of detector defects such as hot pixels. The recorded frames of HD 179949 comprised 4×25 s exposures (see Table 1). Observations of early type Standard stars were also made to enable monitoring of changes in telluric line strength throughout each night. For the first and second nights, the seeing varied in the ranges $0.39''$-$0.97''$ and $0.40''$-$1.4''$ respectively. The seeing was generally $\sim 0.5''$ for observations of HD 179949, while the humidity was very low at 3-8 per cent and 12-20 per cent on each night respectively.

2.1   Data extraction

The worst cosmic ray events were removed at the pre-extraction stage using the Starlink FIGARO routine BCLEAN (Shortridge 1993). The Aladdin-3 arrays used with CRIRES exhibit an odd/even non-linear sensitivity pattern between adjacent columns (i.e. in the cross-dispersion direction) on detectors 1 and 4 and adjacent rows on detectors 2 and 3 (Siebenmorgen & Smette 2008). The effect is not removed by simple flatfielding or nodding between A and B positions and failure to account for this effect results in extracted spectra which display a saw-toothed pattern on a pixel-to-pixel scale. We implemented the method described by Siebenmorgen & Smette (2008) to account for this effect before further extraction of the science frames was carried out. Each spectrum was then extracted by first subtracting the neighbouring frame in and ABBA sequence to eliminate sky background and detector cosmetic effects. This method means that during extraction of the spectra, it is not strictly necessary to model the sky background. However, we fitted low order polynomials (straight line) across the profile at each dispersion position to account for any slight changes in the sky background from exposure to exposure. Due to the dead space between detectors, it is not possible to record a continuous spectrum with CRIRES over a selected wavelength range. We therefore carried out the extraction process in the same manner as we would for four individual orders of a cross dispersed échelle, with the relevant gain and readout noise for each detector.

Table 1. CRIRES/VLT1 observations of HD 179949 for UT 2007 July 26 and August 3.

Object	UT start of first frame	UT start of last frame	Time per exposure [secs]	Number of co-adds per frame	Number of observations	Comments
			UT 2007 July 26/27			
HD 179949	23:51:46	00:06:52	25	4	8	Main F8V Target
HD 182645	00:18:04	00:24:35	50	2	4	B7IV standard
HD 179949	00:39:49	03:26:40	25	4	76	Main F8V Target
HD 158643	00:40:07	03:51:41	10	6	4	A0V Standard
HD 179949	04:04:28	07:54:52	25	4	104	Main F8V Target
HD 212581	08:09:05	08:35:48	50	4	8	B9.5V Standard
HD 212301	08:48:28	09:51:06	50	4	16	F8V target
HD 212581	10:05:19	10:10:31	12	6	4	B9.5 Standard
			UT 2007 Aug 03			
HD 158643	00:18:55	00:23:17	15	4	4	A0V Standard
HD 179949	01:08:19	02:44:18	25	4	44	Main F8V Target
HD 158643	03:05:54	03:17:00	10	6	8	A0V Standard
HD 179949	03:31:11	07:22:23	25	4	104	Main F8V Target
HD 212581	07:39:34	07:53:31	15	6	8	B9.5V Standard
HD 212581	07:56:14	08:36:11	20	6	16	B9.5V Standard
HD 212301	08:49:44	09:35:04	50	4	12	F8V target
HD 212581	09:44:38	10:24:05	20	6	16	B9.5V Standard

The typical gain for a detector is 7 electrons/ADU while the r.m.s readout noise is 10 electrons. The spectra were extracted using ECHOMOP's implementation of the optimal extraction algorithm developed by Horne (1986). ECHOMOP propagates error information based on photon statistics and readout noise throughout the extraction process.

2.2 Wavelength calibration

The wavelength range of our observations was chosen as a compromise between minimising the effects of tellurics, maximising the expected number and strength of planetary spectral lines (See §4) and maximising the expected planet/star flux ratio. Calibration frames using ThAr lamps were taken during the observations, but only yielded typically one or two lines per order in the observed spectral range. We therefore followed the successful approach used in Barnes et al. (2007a,b), where telluric features in the observed spectrum of the standard star were used. A spectrum generated from a HITRAN line list (Rothman et al. 2005) enabled identification of observed features with theoretical wavelengths. A quadratic function was sufficient to describe the nonlinearity between pixel position and the wavelength scale, with between 8 and 23 telluric features used for the spectrum on each of the four detectors. A residual r.m.s. of < 0.042 times the spectrograph resolution element (a $0.4''$ slit is equivalent to 0.429 Å at the mean wavelength of the observations) was obtained resulting in wavelength ranges of $21214.9 - 21330.3$ Å, $21363.0 - 21473.9$ Å, $21503.5 - 21610.2$ Å and $21638.3 - 21740.0$ Å respectively being recorded on each detector.

3 DATA ANALYSIS

3.1 Removal of stellar and telluric spectra

In order to maximise our chances of detecting a signal we first remove contributions from sources which contaminate the planetary spectrum. We have found that the most effective means of removing the stellar and telluric lines involves subtraction of a scaled and shifted master spectrum (Barnes et al. 2007b). For each night of observations, a master spectrum is created by cross-correlating and shifting all observed HD 179949 spectra to the nearest pixel. The resulting spectrum contains an average of the telluric, stellar and planetary signal with the planetary signal smeared out due to its radial velocity variation with orbital phase. The phase ranges over which we chose to observe HD 179949 ensure that any planetary absorption signature will be Doppler shifted from -113 km s^{-1} to +91 km s^{-1} during the planet's orbit about HD 179949.

After subtraction of the master spectrum, the remaining principal variation from spectrum to spectrum is seen as a changing telluric line strength throughout the night due to changes in humidity and airmass of the observed target. The telluric lines thus change their strength relative to the stellar lines, and relative to each other. The consequence of the latter effect is that accurate removal of time varying telluric features can only be carried out effectively when individual lines are resolved, as shown by Bailey et al. (2007). In Barnes et al. (2007b), we fitted the master spectrum to each HD 189733 spectrum in turn by taking derivatives of the spectra and using splines to calculate the scale factor at points across the spectra. This process can account for those lines that behave independently over the night and is described in Collier Cameron et al. (2002) (Appendix A). Care must be taken not to use too few scaling points, which would not adequately account for relative changes in telluric
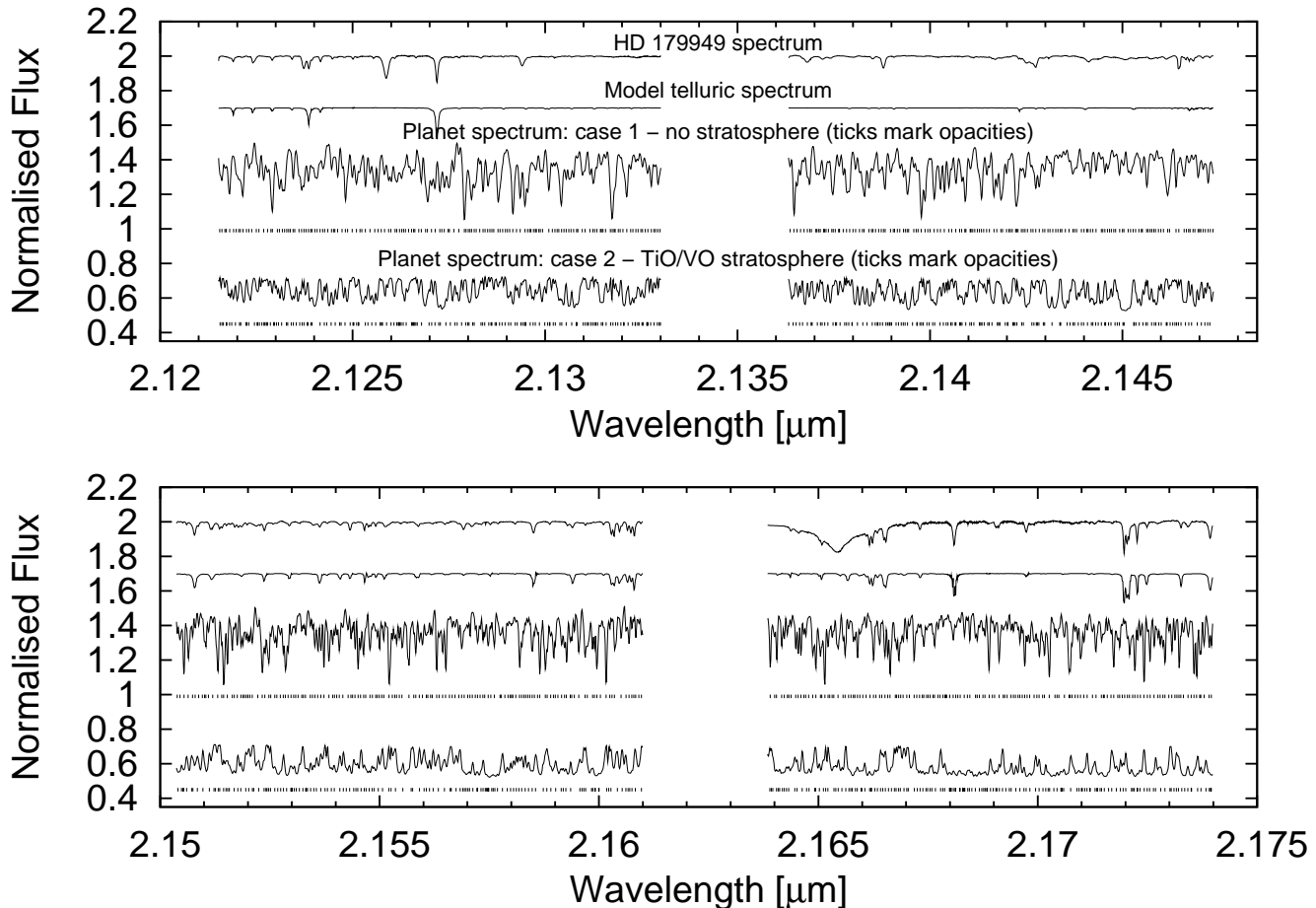
Figure 1. CRIRES wavelength coverage of HD 179949. The four segments (left to right and top to bottom) are the spectral regions recorded on detectors 1 - 4 respectively. Plotted (top to bottom) in each panel are the mean spectrum for 2007 July 26, model telluric spectrum, model planet spectrum with TiO/VO removed (model 1) and model planet spectrum with TiO/VO stratosphere (model 2). For model 2, the transitions are in emission and are weaker relative to the normalised continuum in the 2.120 μm 2.174 μm spectral window. The model spectra have been convolved with a Gaussian to match the instrumental resolution. The tick marks represent opacity wavelengths (before convolution) for each planetary model.

line strength. Conversely, use of too many scaling points could effectively yield a close or perfect match between the individual and master spectrum since the continuum in the master spectrum could be scaled to mimic a weak absorption (e.g. planet) feature. This would result in attenuation or removal of a potential planetary signal. We therefore do not include more scaling points than twice the effective spectral resolution. With these limitations, the effectiveness of our spectrum removal procedure is dependent on spectral resolution, and at the resolution of R ∼ 15,000 (Barnes et al. 2007b) significant residuals inevitably remained. In contrast, the present CRIRES data have R ∼ 50,000, which enable more accurate telluric subtraction.

Some tellurics nevertheless still remain at the 2-σ level (§4) after subtraction of the scaled master spectrum. We therefore reduced the strength of remaining systematics with principal components analysis of the spectral timeseries using the method first described in Collier Cameron et al. (2002) (Appendix B) and discussed in both Barnes et al. (2007a) and Barnes et al. (2007b). The data at fixed wavelength positions are decomposed into a series of eigenvectors

which the main orthogonal trends in the timeseries of observations. Removal of the first four principal components ensure that the remaining systematics due to time varying telluric residuals are subtracted while not significantly attenuating a moving planetary signal. At the high S/N ratios (see §3.2) of the observed spectra, complete reduction of residuals to levels close to 1-σ is not possible.

3.2 Deconvolution and Atmospheric Model

To enable absorption or emission features to be detected, we deconvolve our observed spectra using a model of the planetary atmosphere. In effect, a least squares deconvolution (Donati et al. 1997) is applied to each observed spectrum by using the wavelength positions and line depths of all opacities in the wavelength range of interest (Collier Cameron et al. 1999; Barnes et al. 2007a,b). For HD 179949b, we model an atmosphere with solar metallicity for a temperature, T = 1250 K and surface gravity, log g = 1.33 ms^{-1}. The effective wavelength of the single mean profile is determined by the distribution of line opac-
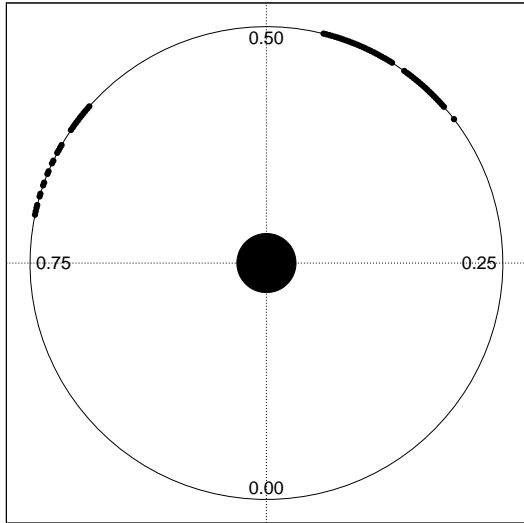
Figure 2. Orbital phase diagram for HD 179949b. Phase 0.00 corresponds to the time of inferior conjunction. The large filled circle at centre represents HD 179949 while the small filled circles represent the phases of observations.

ities, opacity strengths and number of counts at each wavelength (Barnes et al. 1998). The mean weighted effective wavelengths of the deconvolved profiles are $\lambda_c = 2.1434$ μm and $\lambda_c = 2.1428$ μm for model 1 and model 2 respectively. The similarity is a reflection of the uniformity in strength and distribution of opacities in the two scenarios.

We have discussed the sensitivity of the model to mismatches between in the observed and model spectra in Barnes et al. (2007a,b). For detection of absorption/emission features it is necessary that a model with opacities which are as up to date as possible are used. Our models are generated using the Barber et al. (2006) water line list, H_2O being the dominant species in the wavelength region of our observations. We have discussed the role of absorbing species (§1) in the upper atmospheres of those planets which absorb the highest amount of incident solar radiation. For cooler atmospheres, Ti and V are believed to rain out of the upper atmosphere, thereby giving no contribution to emergent spectra. In the case of the hottest CEGPs however, T and V are present as oxides, namely TiO and VO, which absorb incident radiation high in the atmosphere leading to heating and formation of a temperature inversion. It is claimed by Burrows et al. (2008), Burrows et al. (2007) and Knutson et al. (2008) (HD 209458 b) that multi-wavelength mid-infrared observations are in better agreement with this scenario. Fortney et al. (2008) have divided cooler and hotter planets into two regimes which they call pL and pM class respectively. Both Burrows et al. (2008) and Fortney et al. (2008) discuss whether HD 179949 belongs to the former or latter of these classes, but given the relatively early spectral F8-F9V spectral type of HD 179949 itself, it seems likely that HD 179949 belongs to the pM class.

Building upon the work of Barman et al. (2005), model spectra are generated for the two cases (1) where TiO and VO are removed from the atmosphere, leading to dominance of strong bands of H_2O absorption (in the region of interest)

and (2) where TiO and VO lead to formation of a stratosphere, resulting in formation of weak lines in emission (hereafter model 1 and model 2). The form of the spectrum in model 2 is much more blackbody-like than in model 1 and results in an overall lower value for the flux ratio in the wavelength region of our observations. For a fuller description of the model opacities and setup see Ferguson et al. (2005), Barman et al. (2001) and Barman et al. (2005). The resulting models are expected to be very similar to those of Burrows et al. (2008) and Fortney et al. (2008) described above. Fig. 1 shows the mean normalised spectrum from July 26, the model normalised telluric spectrum (Rothman et al. 2005) and the normalised planetary spectra for models 1 and 2.

After co-addition of ABBA sequences, a total of 46 spectra were observed on July 26 and 27 spectra were observed on August 2. The mean S/N ratio, measured from residual ABBA spectra after removal of the template and principal components, was 959 ± 57 and 893 ± 73 for the night of 26 July and 02 August respectively with a combined S/N ratio of 935 ± 71. Deconvolution using model 1 yielded S/N $= 8263 \pm 721$ while model 2 yielded 2589 ± 252, indicating effective gains of 8.84 and 2.77 respectively. The lower S/N achieved through use of model 2 is a consequence of the weaker emission lines (see Fig. 1).

3.3 Matched filter

We aim to isolate the phase dependent planetary absorption signature from the total light of the HD 179949 system. Unlike the stellar spectrum, the planetary spectrum is Doppler shifted due to its orbit and is expected to exhibit a phase variation in strength due to irradiation of its inner face (Barman et al. 2005). The time-dependent changes in Doppler shift and brightness are modelled by using a Gaussian matched filter which has been described in both Barnes et al. (2007a) and Barnes et al. (2007b). The method is a adapted from the reflected light studies which are detailed in Appendix D of Collier Cameron et al. (2002). By modelling the variation in Doppler shifted velocity and planet/star flux ratio (F_p/F_*), we are able, in the presence of a strong detection to determine both the maximum planet/star flux ratio ($\epsilon_0 = F_p/F_*$) and the velocity amplitude of the planet, K_p. Fig. 2 shows the phases at which observations were made. Phases close to $\phi = 0.5$ are favoured because the hot inner face is presented to the observer, resulting in the highest planet/star flux ratios.

3.4 Signal calibration and orbital inclination

The matched filter is calibrated by means of a simulated fake planetary signal with known ϵ_0 and K_p. The fake signal is added to the extracted spectra before further analysis, which involves removal of the mean stellar spectrum and residual noise patterns. As HD 179949 is not a transiting system, the axial inclination of HD 179949 is unknown. However, since Rossiter-McLaughlin effect measurements for a number of systems, including HD 209458 (Bundy & Marcy 2000; Queloz et al. 2000; Winn et al. 2005; Wittenmyer et al. 2005) and HD 189733 (Winn et al. 2006), have shown that the orbital plane of the planet closely matches that of the

axial inclination of the star, we carry out Monte-Carlo simulations to determine the most probable velocity amplitude, K_p, and the orbital inclination, i, of HD 179949b. Using the empirical orbital parameters discussed in section §1, we find most probable values of $K_p = 115$ km s^{-1} and $i = 47.6°$. A matched filter 2D search as described above (§3.3) for the best fitting parameters is scaled to ensure the the planet is recovered at the simulated value of ϵ_0 for the fake planet.

The significance of the result is assessed using bootstrap statistical procedures. The data are re-ordered in a way which randomises the observation phases while preserving the effects of any correlated systematic errors (Collier Cameron et al. 2002). Essentially, the order of the observations is randomised in a set of 3000 trials, thereby scrambling any true planetary signal while enabling the data to retain the ability to produce spurious detections through the chance alignment of systematic errors. The least squares estimate of $log_{10} \epsilon_0$ and associated χ^2 as a function of K_p enable us to plot 68.4, 95.4, 99.0 and 99.9 per cent bootstrap limits on the strength of the planetary signal.

4   RESULTS

We present the results of our search for the 2.143 µm high resolution spectroscopic opacity signatures of HD 179949b in Fig. 3. The timeseries deconvolved spectra spanning both nights of observations are shown in Fig. 3 for model 1 (top left) and model 2 (bottom left). In the former scenario, since the opacities are expected to appear in absorption, a planetary signature would be seen as a dark trail while in the latter scenario, a planetary signature would be seen as a light trail relative to the mean background. In each case, the dashed line represents the velocity path of a planetary signature at the most probable velocity amplitude, $\hat{K}_p = 115$ km s^{-1}, and does not represent a detection.

The dark regions in the χ^2 plots of $log_{10} \epsilon_0$ vs K_p represent local enhancements in χ^2 for particular combinations of parameters. These features are all present within the 68.3, 95.4 per cent confidence (1-2 σ) intervals and are due to systematic features which remain in the residual spectra. It is possible to rule out a number of features where the false alarm probability would be high. An estimate of the upper limit to the velocity amplitude of $K_p(\text{max}) = 155.8 \pm 9.1$ km s^{-1} is determined from the orbital period and semi-amplitude. Planets detected at velocities much in excess of this limit can thus be ruled out. Similarly, a planet with low orbital inclination would be expected to yield a much lower planet/star flux ratio owing to the heated inner face of the planet appearing foreshortened to the observer.

For model 1, we are unable to detect a planetary signal at the most probable velocity amplitude at a level of $log_{10} \epsilon_0 = -3.67$ with 95.4 per cent confidence (2-σ). This equivalent to $F_p/F_* \sim 1/4600$. Similarly, for model 2, we do not detect a planetary signal with $log_{10} \epsilon_0 = -3.30$ ($F_p/F_* \sim 1/2000$) with 95.4 per cent confidence (2-σ). The implications and significance of these results are discussed in §5.

The epoch of inferior conjunction and orbital period (phase, $\phi = 0.0$) of HD 179949 carry uncertainties which may result in significant drift of the phasing by the time of observations. A drift of up to $\pm$ 1hr 18 min or $\phi = \pm 0.0175$

could have accumulated from the ephemeris up to the mid-epoch of the present observations. Since such a drift in observations may be responsible for our inability to detect the planetary signal, we investigated shifting the time of inferior conjunction by ± 15 mins intervals in this range. No clear candidate signature was however detected at any of the shifted ephemerides.

5   DISCUSSION

The significance of our analysis is presented in Fig. 4 which shows the model and observed planet/star flux ratios. Fig. 4 (left) indicates the 99.9, 99, 95.4 and 68.3 per cent upper detection limits for an atmosphere which contains no high altitude absorbing species which lead to a temperature inversion. In this model, only absorption lines are present and our analysis is able to reject this scenario with 99 per cent confidence at a level of $log_{10} \epsilon_0 = -3.53$ ($F_p/F_* \sim 1/3350$) for a planet with the most probable velocity amplitude. The model 2 scenario, where TiO and VO are able to absorb incoming radiation high in the atmosphere and form a temperature inversion, leads to a spectrum resembling a blackbody with weak emission lines superimposed (Fig. 4, right). Since the lines are weak, we are unable to reliably reject this model with our analysis since the 95.4 per cent (2-σ) upper limit of $log_{10} \epsilon_0 = -3.30$ ($F_p/F_* \sim 1/2000$) at the most probable velocity amplitude is higher than the model contrast ratio of $log_{10} \epsilon_0 = -3.46$ ($F_p/F_* \sim 1/2900$) at the mean wavelength of the observations.

Without a clear detection of the signal, it is difficult to constrain the model predictions further since the flux ratio is dependent on the as yet unknown orbital inclination of HD 179949b. The prior distribution for K_p indicates that the relative chance of detecting the planet with $K_p(\text{max})$ (i.e. $i = 90°$) is ~ 9.7 per cent of a detection at $\hat{K}_p$. Similarly, an orbit with i.e. $i = 30°$ carries only a 4.7 per cent relative chance. These extremes are represented in Fig. 4 by the grey spectra which have simply been scaled by the flux expected from the planet at $i = 30°$ and $i = 90°$. Even with $i = 30°$, we can rule out the presence of a planet with a model 1 atmosphere with 99 per cent (marginal) confidence. Conversely, for model 2, were $i = 90°$, we would marginally detect a planet with 99 per cent confidence. There is no evidence for eclipse events in HD 179949b however.

In Barnes et al. (2007a,b), we investigated the effect of model-observation line strength mismatch. However, the transitions of the strongest H_2O lines which contribute to the model spectrum (Barber et al. 2006), and hence the deconvolved spectra, are known experimentally, with significant uncertainties on only the very weakest lines. If we can rule out wavelength and oscillator strength uncertainties in the input H_2O transitions as sources of mismatch between model and observation, uncertainties in line strength may arise from the planetary temperature structure which may be incorrect due to the assumptions of hemispheric-wide hydrostatic equilibrium.

Until a clear detection of a planetary signature is made at high resolution, a quantitative *empirical* model-observation mismatch constraint will not be possible. Nevertheless, successful detection of H_2O at optical (Barman 2007) wavelengths, and of H_2O and CH_4
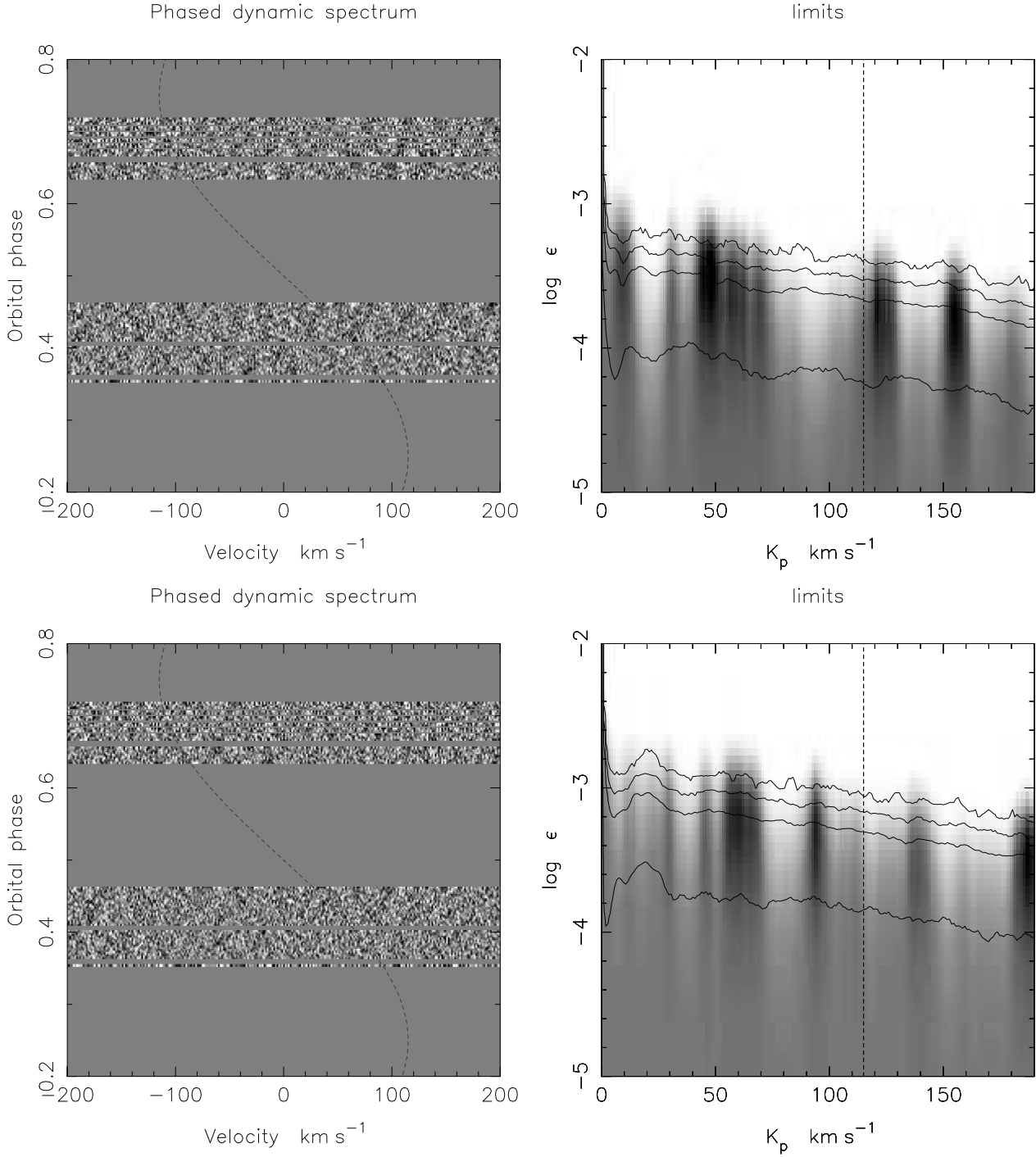
Figure 3. Left: Phased timeseries of the deconvolved residual spectra of HD 179949. The dashed sinusoidal curve represents the *expected* motion of a planetary signal based on the most probable velocity amplitude, $\hat{K}_p = 115$ km s^{-1}. For plotting purposes, all deconvolved profiles have been normalised to the same noise level to optimise the visible information content of the plot. Right: Relative probability χ^2 map of planet-star flux ratio $log_{10} \epsilon_0$ vs K_p. The first 4 principal components have been subtracted from the timeseries spectra. The greyscale in the probability maps represents the probability relative to the best fitting model in the range white for 0 to black for 1. Numerous enhancements in χ^2 result from low level systematic residuals (see main text) which can not effectively be removed. Plotted are the 68.3, 95.4, 99 and 99.9 per cent (bottom to top) confidence levels for a planetary signal detection. No planetary signal is detected at the most probable velocity amplitude, $\hat{K}_p$, which is represented by the vertical dashed line.
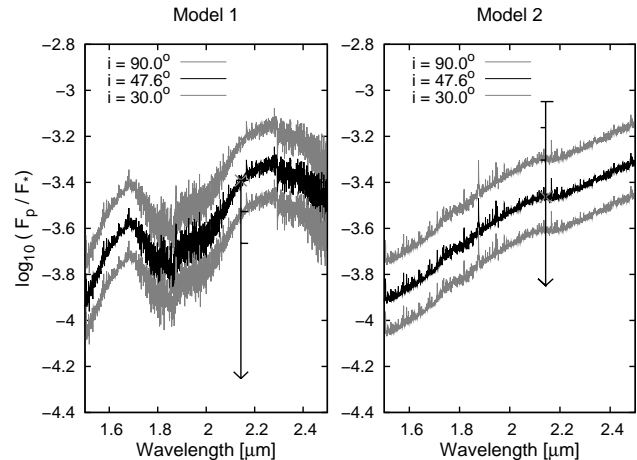
via transmission spectroscopy at mid-infrared wavelengths (Tinetti et al. 2007b; Swain et al. 2008), have relied upon models (Tinetti et al. 2007a) which contain reliable molecular opacities such as the H_2O transitions of Barber et al. (2006). The mid-infrared observations of the spectral energy distribution of HD 189733b by Tinetti et al. (2007b) and Swain et al. (2008) rely on relatively broad spectral regions where the match between observation and model appears to be very close. While transmission spectroscopy is sensitive to the planetary atmospheric signature at the terminator, the same opacities are included in the model we have used for our dayside average spectrum, and have been used by Barman (2008), to infer the presence of H_2O and CO in the atmosphere of HD 189733b.

Our inability to detect H_2O (the only species in the wavelength interval of our observations) in the atmosphere of HD 179949b, can be explained by the expected model 2 scenario and lack of required sensitivity in our data. On the other hand, for HD 189733b, we rejected the expected model 1 scenario (Barnes et al. 2007b) using the same technique as presented in this paper. This may be explained by a lower than expected contrast ratio resulting from efficient flux redistribution at the deeper layers probed by shorter wavelengths (Barman 2008). This could also apply to our rejection of the model 1 scenario for HD 179949b. However, given the earlier spectral type of HD 179949 when compared with HD 189733, and subsequent higher irradiation of HD 179949b, as already discussed, the model 2 scenario seems more appropriate (Fortney et al. 2008; Burrows et al. 2008). It is worth noting that the deeper atmospheric layers probed by the shorter wavelength observations in the model 1 scenario may be blocked by the presence of the high altitude absorber(s) in the model 2 scenario. Hence a non-detection of HD 179949b with higher S/N ratio observations could not be explained in the same way as for HD 189733b.

6   CONCLUSION

We have applied a planetary atmospheric model with two physically different conditions in an attempt to detect the planetary signature of HD 179949b. We are able to reject the scenario in which Ti and V are depleted from the atmosphere of HD 179949b in agreement with the predictions of recent models. We have also assessed our ability to test the models in which TiO and VO are present in the upper atmosphere, resulting in a temperature inversion and lines appearing in emission. We are however unable to detect a planet using this model, or to reject the model since our data do not achieve the necessary S/N ratios required. The 99 per cent confidence limit is 2 times higher than the expected flux ratio at the most probable velocity amplitude of the planet and would thus necessitate a further six nights of observation before this level of sensitivity could be reached.

In order to reliably test the most recent models which include a stratosphere and weak emission, cross dispersed spectrographs which offer greater wavelength coverage will afford higher S/N gain and thus improve our chances of detection. Equally, study of transiting systems reduce the degeneracy considerably in any analysis since the inclination is known and will be close, or equal to $90°$. The greater maximum brightness of a transiting CEGP system will increase our chances of detecting and characterising the planet.

Figure 4. Model and 2.14 µm planet/Star flux ratios for HD 179949b. Shown are models for model 1, absorption (left) and model 2, TiO/VO stratosphere, emission spectrum (right). Some apparent emission features are due to *stellar absorption* lines and result from dividing the planet spectrum by the stellar spectrum. The black crosses indicate the mean model flux over the wavelength of observations for the most probable inclination. Upper limits corresponding to the levels in Fig. 3 (99.9, 99 and 95.4 per cent) are marked by horizontal bars (from top to bottom) for our analysis using each model. The 99.9 per cent observational upper limit is coincident with the mean flux level for the model 1 model. The width of the top horizontal bar in each case (99.9 per cent confidence) represents the wavelength range of the CRIRES spectroscopic observations. For model 1, we can marginally exclude the model with 99.9 per cent confidence at the most probable inclination of $47.6°$. For model 2 we are unable to exclude the model since the 95.4 per cent confidence level (2-sσ) is above the model flux ratio and artifacts are present between 2-sσ and 1-sσ (68.3 per cent confidence marked by the arrow).

REFERENCES

Bailey J., Simpson A., Crisp D., 2007, PASP, 119, 228
Barber R. J., Tennyson J., Harris G. J., Tolchenov R. N., 2006, MNRAS, 368, 1087
Barman T., 2007, ApJ, 661, L191
Barman T. S., 2008, ApJ, 676, L61
Barman T. S., Hauschildt P. H., Allard F., 2001, ApJ, 556, 885
Barman T. S., Hauschildt P. H., Allard F., 2005, ApJ, 632, 1132

Barnes J. R., Barman T. S., Prato L., Segransan D., Jones H. R. A., Leigh C. J., Collier Cameron A., Pinfield D. J., 2007, MNRAS, 382, 473

Barnes J. R., Collier Cameron A., Unruh Y. C., Donati J. F., Hussain G. A. J., 1998, MNRAS, 299, 904

Barnes J. R., Leigh C. J., Jones H. R. A., Barman T. S., Pinfield D. J., Collier Cameron A., Jenkins J. S., 2007, MNRAS, 379, 1097

Bundy K. A., Marcy G. W., 2000, PASP, 112, 1421

Burrows A., Budaj J., Hubeny I., 2008, ApJ, 678, 1436

Burrows A., Hubeny I., Budaj J., Knutson H. A., Charbonneau D., 2007, ApJ, 668, L171

Butler R. P., Wright J. T., Marcy G. W., Fischer D. A., Vogt S. S., Tinney C. G., Jones H. R. A., Carter B. D., Johnson J. A., McCarthy C., Penny A. J., 2006, ApJ, 646, 505

Collier Cameron A., Horne K., Penny A., James D., 1999, Nature, 402, 751

Collier Cameron A., Horne K., Penny A., Leigh C., 2002, MNRAS, 330, 187

Cowan N. B., Agol E., Charbonneau D., 2007, MNRAS, 379, 641

Donati J.-F., Semel M., Carter B., Rees D. E., Collier Cameron A., 1997, MNRAS, 291, 658

Eggenberger A., Udry S., Chauvin G., Beuzit J.-L., Lagrange A.-M., Ségransan D., Mayor M., 2007, A&A, 474, 273

Ferguson J. W., Alexander D. R., Allard F., Barman T., Bodnarik J. G., Hauschildt P. H., Heffner-Wong A., Tamanai A., 2005, ApJ, 623, 585

Fortney J. J., Lodders K., Marley M. S., Freedman R. S., 2008, ApJ, 678, 1419

Harrington J., Hansen B. M., Luszcz S. H., Seager S., Deming D., Menou K., Cho J. Y.-K., Richardson L. J., 2006, Science, 314, 623

Harrington J., Luszcz S., Seager S., Deming D., Richardson L. J., 2007, Nature, 447, 691

Horne K. D., 1986, PASP, 98, 609

Knutson H. A., Charbonneau D., Allen L. E., Burrows A., Megeath S. T., 2008, ApJ, 673, 526

Queloz D., Eggenberger A., Mayor M., Perrier C., Beuzit J. L., Naef D., Sivan J. P., Udry S., 2000, A&A, 359, L13

Richardson L. J., Deming D., Seager S., 2003, ApJ, 597, 581

Rothman L. S., Jacquemart D., Barbe A., +25 co-authors 2005, Journal of Quantitative Spectroscopy and Radiative Transfer, 96, 139

Santos N. C., Israelian G., Mayor M., 2004, A&A, 415, 1153

Shkolnik E., Walker G. A. H., Bohlender D. A., 2003, ApJ, 597, 1092

Shortridge K., 1993, in ASP Conf. Ser. 52: Astronomical Data Analysis Software and Systems II The Evolution of the FIGARO Data Reduction System. pp 219–+

Siebenmorgen R., Smette A., 2008, Very Large Telescope, Science Operations, CRIRES User Manual. European Southern Observatory (http://www.eso.org/instruments/crires/doc)

Swain M. R., Vasisht G., Tinetti G., 2008, Nature, 452, 329

Tinetti G., Liang M.-C., Vidal-Madjar A., Ehrenreich D., Lecavelier des Etangs A., Yung Y. L., 2007, ApJ, 654, L99

Tinetti G., Vidal-Madjar A., Liang M.-C., Beaulieu J.-P., Yung Y., Carey S., Barber R. J., Tennyson J., Ribas I., Allard N., Ballester G. E., Sing D. K., Selsis F., 2007, Nature, 448, 169

Tinney C. G., Butler R. P., Marcy G. W., Jones H. R. A., Penny A. J., Vogt S. S., Apps K., Henry G. W., 2001, ApJ, 551, 507

Winn J. N., Johnson J. A., Marcy G. W., Butler R. P., Vogt S. S., Henry G. W., Roussanova A., Holman M. J., Enya K., Narita N., Suto Y., Turner E. L., 2006, ApJ, 653, L69

Winn J. N., Noyes R. W., Holman M. J., Charbonneau D., Ohta Y., Taruya A., Suto Y., Narita N., Turner E. L., Johnson J. A., Marcy G. W., Butler R. P., Vogt S. S., 2005, ApJ, 631, 1215

Wittenmyer R. A., Endl M., Cochran W. D., 2007, ApJ, 654, 625

Wittenmyer R. A., Welsh W. F., Orosz J. A., Schultz A. B., Kinzel W., Kochte M., Bruhweiler F., Bennum D., Henry G. W., Marcy G. W., Fischer D. A., Butler R. P., Vogt S. S., 2005, ApJ, 632, 1157

Wolf M., Harmanec P., 2004, Informational Bulletin on Variable Stars, 5575, 1